



**HAL**  
open science

## Thermochromic properties of pure NiTiO<sub>3</sub> and its Cu- or Co-doped derivatives

Loren Acher, Hyewon Ji, Nicolas Garino, Florian Massuyeau, Laurie Pontille, François Cauwet, Arnaud Brioude, Stéphane Jobic, Gabriel Ferro, Davy Carole

► **To cite this version:**

Loren Acher, Hyewon Ji, Nicolas Garino, Florian Massuyeau, Laurie Pontille, et al.. Thermochromic properties of pure NiTiO<sub>3</sub> and its Cu- or Co-doped derivatives. *Ceramics International*, 2023, 49 (8), pp.12267-12273. 10.1016/j.ceramint.2022.12.079 . hal-03921687

**HAL Id: hal-03921687**

**<https://cnrs.hal.science/hal-03921687>**

Submitted on 9 Mar 2023

**HAL** is a multi-disciplinary open access archive for the deposit and dissemination of scientific research documents, whether they are published or not. The documents may come from teaching and research institutions in France or abroad, or from public or private research centers.

L'archive ouverte pluridisciplinaire **HAL**, est destinée au dépôt et à la diffusion de documents scientifiques de niveau recherche, publiés ou non, émanant des établissements d'enseignement et de recherche français ou étrangers, des laboratoires publics ou privés.

## Thermochromic properties of pure NiTiO<sub>3</sub> and its Cu- or Co-doped derivatives

Loren Acher<sup>1</sup>, Hyewon Ji<sup>1</sup>, Nicolas Garino<sup>1</sup>, Florian Massuyeau<sup>2</sup>, Laurie Pontille<sup>1</sup>, François Cauwet<sup>1</sup>, Arnaud Brioude<sup>1</sup>, Stéphane Jobic<sup>2</sup>, Gabriel Ferro<sup>1</sup>, Davy Carole<sup>1\*</sup>

<sup>1</sup>Laboratoire Multimatériaux et Interfaces, UMR CNRS 5615, Université Claude Bernard Lyon 1, France

<sup>2</sup>Nantes Université, CNRS, Institut des Matériaux de Nantes Jean Rouxel, F-44000 Nantes, France

\*Corresponding author.

E-mail address: [davy.carole@univ-lyon1.fr](mailto:davy.carole@univ-lyon1.fr)

Phone number: +334 26 23 45 24

Postal address: Université Lyon 1

Laboratoire des Multimatériaux et Interfaces

Bat Chevreul, 6 rue Victor Grignard

69622 Villeurbanne CEDEX

### Abstract:

Nickel titanate is a yellow-brown pigment which adopts the ilmenite crystal structure as corundum and hematite. Since Cr doped Al<sub>2</sub>O<sub>3</sub> and Fe<sub>2</sub>O<sub>3</sub> present a thermochromic behaviour, NiTiO<sub>3</sub> was also studied for its potential ability to change colour with temperature. Powders were synthesized via a modified Pechini method followed by a calcination step at 700 °C. The thermochromic properties in the 20 °C – 400 °C temperature range were collected via the determination of the colorimetric L\*a\*b\* parameters. Namely, the hue continuously shifts from yellow-brown to red-brown, with L\*a\*b\* parameters moving from 60.4/19.2/58.5 to 42.9/30.5/43.1. This color change is fully reversible even after several cycling. Temperature dependent UV-vis spectroscopy showed that the transparency window at 550 - 650 nm at room temperature shifts to 575 - 650 nm at 400 °C. This fully explains the observed colour change. Finally, the effects of Cu or Co doping on NiTiO<sub>3</sub> optical and thermochromic properties were also investigated.

**Key words:** Thermochromism, C. Optical properties, C. Colour, D. BaTiO<sub>3</sub> and titanates

## 1. Introduction

Thermochromism refers to the ability of matter to undergo a colour change vs. temperature. Thermochromic materials are potentially used in a wide range of applications such as temperature memory sensors (cold chain break sensor, threshold temperature sensor for aeronautic application...), temperature sensors for safety (kitchen tools...), smart materials for specific application (smart windows or concrete for building energy efficiency...) or in day-to-day life as smart pigment (textile, ink, packaging...) [1-4]. Colour change with temperature variation can be reversible or irreversible, and continuous (gradual change in colour) or discontinuous (sudden change in colour). In the case of inorganic thermochromic compounds [5], the colour change can be due to a chemical composition alteration (e.g. dehydration, decarbonation, decomposition) [6] leading then to an irreversible change. In contrast, reversibility may be obtained with phase transition [7-10], band gap shrinkage [11] and/or change in the ligand field [12] since the integrity of the material is not affected at very first sight. In order to choose the best suited material for the desired thermochromic application, the main properties to consider are the initial colour, the transition temperature range, the colour contrast and the reversibility/cyclability if needed.

Among the reversible inorganic thermochromic material, hematite  $\alpha\text{-Fe}_2\text{O}_3$  is well-known. It has a reddish brown colour coming from two  $2p(\text{O}^{2-}) \rightarrow 3d(\text{Fe}^{3+})$  charge transfers [13]. Upon heating, the thermal expansion results in an increase of the metal-oxygen bonds distances [14, 15]. The evolution of the local environment of  $\text{Fe}^{3+}$  sites (size and degree of distortion) with increasing temperature leads to a change in the positioning of iron energy levels, which results in red shift of the optical absorption and so to thermochromic property. In the case of  $\alpha\text{-Al}_2\text{O}_3$ , which is isostructural to  $\text{Fe}_2\text{O}_3$ , Cr doping gives a red colour to the crystal at room temperature and it turns to green upon heating [16]. This colour change is explained by a decrease of the crystal field strength with increasing temperature, which induces a downward shift in energy of the parity forbidden but spin allowed  ${}^4\text{A}_2 \rightarrow {}^4\text{T}_2$  and  ${}^4\text{A}_2 \rightarrow {}^4\text{T}_1$  electronic transitions.

NiTiO<sub>3</sub> is a yellow-brown pigment reported as a semiconductor with an optical gap around 2.2 eV and Ni<sup>2+</sup> cations anti-ferromagnetically coupled. It adopts the ilmenite crystalline structure, i.e. the same as  $\alpha$ -Fe<sub>2</sub>O<sub>3</sub> and  $\alpha$ -Al<sub>2</sub>O<sub>3</sub> and is actively studied for photocatalytic and multiferroic applications [17-19] but not for thermochromic ones. Due to the above-mentioned structural similarities with known thermochromic compounds and the fact that NiTiO<sub>3</sub> is already naturally coloured at room temperature, we suspect that NiTiO<sub>3</sub> could also be thermochromic. This will be investigated in the present study. Besides, since metal doping of this compound is known to change its colour [20], we also investigate the effect of partial Ni substitution by Cu and Co on optical properties, and specifically on the thermochromism colour rendering. These elements were chosen due to their effective ionic radius, close to the one of Ni: Cu<sup>2+</sup> (0.73 Å), Co<sup>2+</sup> (0.745 Å) and Ni<sup>2+</sup> (0.690 Å) (high spin configuration, coordination number: six) [21]. Such radius similarity explains why their insertion on Ni site is easy, as already observed by Guet *et al.* for copper in the range 0 – 20 at.% [22]. In our case, the doping rate was limited to 2 at.% to prevent the formation of secondary phases that could trigger undesired darkening of the product.

## 2. Material and methods

### 2.1. Materials preparation

NiTiO<sub>3</sub>, Ni<sub>1-x</sub>Cu<sub>x</sub>TiO<sub>3</sub> and Ni<sub>1-x</sub>Co<sub>x</sub>TiO<sub>3</sub> powders were synthesized via a modified Pechini method (protocol adapted from [23]). Typically, for pure NiTiO<sub>3</sub> sample, 3.88 g of nickel(II) nitrate (97 %, Fluka), 4.40 g of titanium(IV) *n*-butoxide (97 %, Sigma-aldrich) and 5 g of citric acid (99 %, Alfa Aesar) were first separately dissolved in 20 ml of ethanol. The citric acid solution was then added drop by drop to the Ti<sup>4+</sup> solution (the resulting solution remained translucent). After 10 min of homogenization under stirring at room temperature (RT), the Ni<sup>2+</sup> solution was finally added in order to form the metal-citrate complex (the solution still remained translucent). The overall solution was then heated at 90 °C in a water bath until the complete evaporation of the solvent and the formation of a green coloured gel. The as obtained precursor was first calcined

at 300 °C during one hour, and second heated at 700 °C during three hours in air. After cooling to room temperature, a yellow-brown NiTiO<sub>3</sub> powder was achieved.

Ni<sub>0.98</sub>Cu<sub>0.02</sub>TiO<sub>3</sub> and Ni<sub>0.98</sub>Co<sub>0.02</sub>TiO<sub>3</sub> were prepared with copper(II) nitrate (99 %, Carl Roth) and cobalt(II) nitrate (98 %, Carl Roth) as precursors, respectively. The protocol was the same as for pure NiTiO<sub>3</sub>, the precursors being dissolved separately in ethanol and the amount of Ni precursor being adjusted according to the desired amount of dopant. Typically, for the same above mentioned proportion of Ti and citric acid in 20 ml of ethanol each, 3.71 g of Ni, 0.063 g of Cu or 0.075 g of Co precursors were dissolved in 20, 10 and 10 ml of ethanol respectively. The as-prepared solutions containing dopant ions were then added in the Ni/Ti solution, just after the Ni<sup>2+</sup> addition.

## *2.2 Sample characterization*

High-Temperature X-Ray Diffraction (HT-XRD) was performed using a Panalytical diffractometer (X'Pert Pro MPD) equipped with an external heating chamber provided by Anton Paar (HTK 1200N). A fast detector (PIXcel 1D), in the Bragg Brentano geometry, and a copper anode (wavelength (Cu K<sub>α</sub>): 1.5419 Å) were used. All data were collected using the same conditions, in the angular range  $12 < 2\theta < 100^\circ$ , with step intervals of  $0.026^\circ$  (in  $2\theta$ ) and a scan set time of 21 minutes (scan rate of  $4.2^\circ/\text{min}$ ). Measurements were done first at RT, then from 100 °C up to 400 °C with a step of 50 °C and finally after Back to Room Temperature (BRT). Phase identification and structural analysis (Rietveld refinements [24]) were performed using the Match! software (version 3, Crystal Impact) and the Crystallography Open Database.

Morphologies characterizations were performed by Field-Emitter Scanning Electron Microscopy (FE-SEM) in a Zeiss Merlin VP Compact apparatus using an accelerating voltage of 1 kV.

A homemade set-up was used for both qualitative and quantitative colour estimation in combination with heating and with the advantage of allowing a direct visualisation of the colour

evolution in temperature (Fig.SI.1). It is composed of a heating stage (thermocouple-controlled) positioned inside a closed black box and uniformly illuminated from the top using commercial white light-emitting diodes which simulate the daylight (light temperature 5500 K). An external camera (Canon EOS 550D) equipped with a macro lens (EF-S 24mm f/2.8 STM), perpendicular to the observed sample, was used in order to take pictures from the top side after reaching the targeted temperature. Pictures were taken at RT, 50 °C and from 100 °C up to 400 °C every 25 °C. In order to evaluate thermochromism reversibility, pictures were also taken after cooling BRT. For reproducibility reasons, samples were put on a dull white boron nitride crucible. It thus avoids both chemical reactivity with the metallic heating stage and metallic reflection of the light on the heating stage, which could induce colour estimation errors. A white reference material (barite BaSO<sub>4</sub> pellet) was also placed outside of the heating stage but still in the photography-captured area for image treatment. After adjusting the white balance colour using BaSO<sub>4</sub>, the L\*, a\*, b\* CIELAB colour parameters of the studied powders were extracted from the photographs using GIMP (Gnu Image Manipulation Program) software (2.10 version), considering an average area of 30x30 pixels taken on the powder. CIELAB is a three-dimensional colour space where L\* is a measure of lightness (100 = white, 0 = black), and a\* and b\* are colour parameters (-a\* = green, +a\* = red; -b\* = blue, + b\* = yellow with a\* and b\* ranging from - 120 to + 120). The colour difference, i.e. colour contrast, between room temperature and the measured temperature ( $\Delta E$ ) was determined using the following formula:

$$\Delta E = \sqrt{(L_T^* - L_{RT}^*)^2 + (a_T^* - a_{RT}^*)^2 + (b_T^* - b_{RT}^*)^2}$$

with L<sub>T</sub><sup>\*</sup>, a<sub>T</sub><sup>\*</sup> and b<sub>T</sub><sup>\*</sup> the CIELAB parameters at the measured temperature, and L<sub>RT</sub><sup>\*</sup>, a<sub>RT</sub><sup>\*</sup> and b<sub>RT</sub><sup>\*</sup> the CIELAB parameters at room temperature. Let us mention that a color difference leading to 1 <  $\Delta E$  < 2 can only be detected by an experienced observer. For an unexperienced observer,  $\Delta E$  has to be higher than 2. From  $\Delta E$  above 3.5, a clear colour difference is noticed by anyone [25].

Room-temperature UV-visible diffuse reflectance spectra were recorded on a Perkin Elmer UV-NIR 1050+ spectrophotometer equipped with an integrating sphere coated with Spectralon. For temperature-resolved measurements, a praying mantis accessory from Harrick equipped with a high temperature reaction chamber (UV-Vis-NIR) (HVC-VUV-5) was used. This setup was installed inside the 1050+ photospectrometer. The reflectance values were measured from 200 to 1200 nm at 1 nm intervals. The spectra were recorded every 25 °C up to 250 °C. The Kubelka-Munk equation ( $KM = \frac{(1-R)^2}{2R}$ , with R the reflectance at a given wavelength) was used to transform diffuse reflection spectra into absorption ones.

### 3. Results and discussion

#### 3.1 Pure NiTiO<sub>3</sub>

Nickel titanate adopts the ilmenite structure type (R-3c space group) [26-28]. The XRD pattern of undoped NiTiO<sub>3</sub> sample recorded at room temperature was indexed with the COD (Crystallography Open Database) card no. 1544718 [27] and is in perfect accordance with the expected ilmenite structure (Fig. 1a, top). Considering the full width at half maximum (FWHM) of the diffraction peaks, an average crystallite size L of 55 nm was estimated using Scherrer's formula:

$$L = \frac{K \times \lambda}{FWHM \times \cos\theta}$$

where K is the Scherrer constant (= 0.94),  $\lambda$  the wavelength of the radiation and  $\theta$  the diffraction angle of the peak. Here, crystallite means a coherent scattering domain, which is, of course, different from the grain observable by SEM. Indeed, SEM pictures show that NiTiO<sub>3</sub> powder is composed of micrometric agglomerates made of 30 – 120 nm large grains (Fig. 2) which decently correlates with Scherrer's formula results.

Considering now the other XRD patterns of Figure 1a, recorded with increasing temperature, no phase transformation can be detected in the range 25 – 400 °C. The main effect of temperature is limited to a slight shift of all the peaks towards smaller  $2\theta$  angles (this is better shown in Figure 1b), corresponding to an increase of crystal cell volume with temperature, as expected from thermal expansion. When estimating the separate effects for a and c parameters, one can evidence a slight anisotropy in thermal expansion: c parameter increases more rapidly than a one (Figure 3). This leads to a linear increase of the c/a ratio with temperature, being found 0.07% higher at 400 °C as compared to RT value (calculated as follow:  $\delta(c/a)/(c/a)$  (%)). These experimental data are in good agreement with the ones already reported by Boysen *et al.* who determined a variation of c/a ratio of 0.1 % between 27 and 427 °C [29].

Coming now to the optical properties of pure NiTiO<sub>3</sub>, Kubelka-Munk transformed reflectance spectra collected from RT to 400 °C are depicted in Figure 4 in the 300-800 nm interval. The overall shape of the absorption spectra is very similar to those reported in the literature [22, 30-32] namely with three observable domains.

A broad absorption takes place at 450 nm and at the highest wavelengths (>740nm) due to respectively Ni on site the  ${}^3A_{2g}(F) \rightarrow {}^3T_{1g}({}^3P)$  and  ${}^3A_{2g} \rightarrow {}^3T_{1g}({}^3F)$  spin-allowed transitions. Absorption shoulders observed around 510 and 740 nm can be attributed respectively to spin-forbidden transitions  ${}^3A_{2g}(F) \rightarrow 1A_{1g}({}^1G)$  and  ${}^3A_{2g}(F) \rightarrow {}^1T_{2g}({}^1D)$  in one part and  ${}^3A_{2g} \rightarrow {}^1E_g({}^1D)$  in the other part. At lowest wavelengths (320- 400 nm), the O<sup>2-</sup> - Ti<sup>4+</sup> (250 – 320 nm) and O<sup>2-</sup> - Ni<sup>2+</sup> (320 -390 nm) charge transfers can explain the absorption bands. In the 400-600 nm window, the  ${}^3A_{2g}(F) \rightarrow {}^3T_{1g}({}^3P)$ ,  ${}^3A_{2g}(F) \rightarrow 1A_{1g}({}^1G)$  and  ${}^3A_{2g}(F) \rightarrow {}^1T_{2g}({}^1D)$  transitions are overlapped. The former, spin allowed, is much more intense than the two latter that are spin forbidden. When temperature increases, a down shift is observed for the  ${}^3A_{2g}(F) \rightarrow {}^3T_{1g}({}^3P)$  that will progressively overlap the  ${}^3A_{2g}(F) \rightarrow 1A_{1g}({}^1G)$  and  ${}^3A_{2g}(F) \rightarrow {}^1T_{2g}({}^1D)$  ones as predicted by the Tanabe-Sugano diagram associated for a d<sup>8</sup> configuration of Ni in octahedral site [33]. At the end, the absorption



at wavelengths lower than 400 nm is associated to charge transfer transitions. Namely  $\text{Ni}^{2+}$  to  $\text{Ti}^{4+}$ ,  $\text{O}^{2-}$  to  $\text{Ni}^{2+}$  and  $\text{O}^{2-}$  to  $\text{Ti}^{4+}$  charge transfer may compete, the two first lying a priori at lower energy than the latter, Ni-d levels contributing both to the top and the bottom of the valence and conduction band built respectively on O-sp and Ti-d orbitals. As common, position of charge transfers is significantly impacted by temperature due to change in the orbital overlap. Let us notice that the assignment of the absorption bands may differ with authors. Hence, the band occurring in the blue region is assigned to a Ni - Ti charge transfer by Rossman [30], the observed shoulders being related to a splitting of the Ti-d block. Nevertheless, we may notice that the absorption at about 2.2 eV disappears for  $\text{NiTiO}_3$  prepared as thin films suggesting that this band is associated rather to parity forbidden d-d transition than to a charge transfer, the difference in the oscillator strength between the two transition type being of several orders of magnitude. Whatever, the transparency window shifts roughly from 550 - 650 nm to 575 - 650 nm going from RT to 400 °C. This fully explains the colour change from yellow-brown to red-brown, two colours far from being saturated.

In order to get quantitative information about the effective thermochromism of  $\text{NiTiO}_3$  material, the  $L^*a^*b^*$  parameters were determined as a function of temperature using our homemade setup (see Table 1). First of all,  $\text{NiTiO}_3$  is clearly a thermochromic material, changing from yellow-brown at room temperature to darker brown at 400 °C (Table 1).  $L^*$  and  $b^*$  parameters both decrease whereas  $a^*$  increases with temperature. The colour change, i.e. the thermochromism, is continuous and totally reversible as  $L^*a^*b^*$  parameters come back to their original values when BRT (see bottom of Table 1). This was repeated up to 10 times without significant change of the results. Colour contrast  $\Delta E$ , calculated from these data, was used to further quantify the thermochromism of  $\text{NiTiO}_3$  (Fig. 5). The progressive increase of  $\Delta E$  with temperature confirms that the phenomenon is continuous. The maximum value obtained at 400 °C is  $\sim 26$ , which is clearly detectable by human eyes. When comparing with  $\Delta E$  values reported in the literature for other yellowish (at RT) thermochromic compounds, i.e.  $\text{Y}_3\text{Fe}_5\text{O}_{12}$  and

$\text{CaZr}_4(\text{P}_{0.95}\text{V}_{0.05}\text{O}_4)_6$ , we can see that  $\text{NiTiO}_3$  is less thermochromic than  $\text{Y}_3\text{Fe}_5\text{O}_{12}$  ( $\Delta E \sim 24$  in the 25 - 255 C range [12] while we obtained  $\Delta E = 17.5$  for  $\text{NiTiO}_3$  in the same range) but more thermochromic than  $\text{CaZr}_4(\text{P}_{0.95}\text{V}_{0.05}\text{O}_4)_6$  ( $\Delta E \sim 4.1$  in the 30 – 170°C range [34] versus  $\Delta E = 12$  for our  $\text{NiTiO}_3$  in the same range).

Note that the few values of  $L^*a^*b^*$  parameters for pure  $\text{NiTiO}_3$  (at RT) which can be found in the literature are quite different from our results [32]. These parameters were found to vary, depending on calcination temperature (750 – 950 °C), in the range  $71.41 < L^* < 74.6$ ,  $3.07 < a^* < 8.16$  and  $38.48 < b^* < 42.41$ . Note that our samples were calcined at lower temperature (700 °C) than in this study, which can explain these  $L^*a^*b^*$  differences. Despite this, these reported CIELAB parameters leads to rather close yellow/brown hues as compared to the ones of our samples.

Having evidenced for the first time the thermochromism of undoped  $\text{NiTiO}_3$ , we extended the study to the effect of dopant addition on this colour change.

### 3.2 Cu and Co-doped $\text{NiTiO}_3$

The purity of the 2 % Cu and Co-doped samples was checked by XRD. No secondary phase containing copper or cobalt was detected while slight excess of NiO (bunsenite, COD card no. 9008693) and/or  $\text{TiO}_2$  (rutile, COD card no. 9009083) were found which depended on the type of sample. For Co-doping, 1.9 weight % of  $\text{TiO}_2$  and < 1 weight% of NiO was obtained. For Cu doping, only  $\text{TiO}_2$  in excess of 2.0 weight% was detected. Note that  $\text{TiO}_2$  and NiO traces are often formed during  $\text{NiTiO}_3$  synthesis, even in undoped sample [22, 35]. These two phases were also found randomly in some undoped powders but we did not notice any detectable impact of these phases on the colour of the synthesized powders. Indeed, the obtained  $L^*a^*b^*$  parameters were found identical in the uncertainty range compared to an undoped “pure” sample.

The addition of 2 mol % Cu in  $\text{NiTiO}_3$  structure induces a colour change at room temperature from yellow-brown to brown (Table 2). This colour change can be correlated to the evolution of the UV-Vis reflectance spectrum which clearly shifts toward lower reflectance values on the

entire visible range when doping with Cu (Fig. 6). Also, the reflection band centered around 580 nm for undoped NiTiO<sub>3</sub> is shifted to lower energy (~600 nm) after Cu doping. This shift to lower energy was also observed by Guiet *et al.* but for higher doping level ( $\geq 5\%$ ) [22]. Both effects correlate well with the brownishing/darkening of the powder colour due to higher red contribution and overall higher absorption of visible light.

Interestingly, in the case of Co-doped NiTiO<sub>3</sub>, the change in colour is more pronounced since the powder becomes now greenish with 2 mol % Co doping (Table 2). Here, a clear absorption band appears around 600 nm, which could be attributed to the  ${}^4T_{1g} \rightarrow {}^4T_{1g}(P)$  transition of Co<sup>2+</sup> in an octahedral site [36]. It reduces the yellow contribution of the colour and thus shifts it towards the green (Fig. 6).

Finally, the colorimetric and thermochromic properties of these Cu and Co-doped samples were evaluated (see Fig. 7 and Tables 2 & 3). Alike for undoped NiTiO<sub>3</sub>, all doped samples show a reversible thermochromism in the range 20 – 400 °C. Despite generating different colors at RT, both Cu and Co doping lead to similar dark brownishing at 400 °C. Their  $\Delta E$  evolution with temperature is also very similar but always lower than for undoped material. This means that doping with Cu or Co have negative impact on the thermochromic properties of NiTiO<sub>3</sub>, even though the case of Co doping is intrinsically interesting since it shifts the RT colour towards green.

#### 4. Conclusion

Nickel titanate was synthesized using modified Pechini method using nickel nitrate and titanium(IV) n-butoxide. The undoped powder exhibits a thermochromic behavior with a  $\Delta E$  regularly increasing up to 26 at 400 °C. When doping with Cu or Co elements, such thermochromism decreases in both cases. Co doping leads to greeninshing of the powder while Cu doping leads to brownishing.

## Acknowledgments

The authors would like to thank the CT $\mu$  platform for SEM characterizations and the CMTC Grenoble-INP platform for XRD measurements. The authors are very grateful to S. Coindeau and T. Encinas for fruitful discussions.

## Declaration of competing interest

The authors declare that they have no known competing financial interests or personal relationships that could have appeared to influence the work reported in this paper.

## Funding sources

This research did not receive any specific grant from funding agencies in the public, commercial, or not-for-profit sectors.

## References

- [1] M.A. White, M. LeBlanc, Thermochromism in commercial products, *J. Chem. Educ.*, 76 (1999) 1201, <https://doi.org/10.1021/ed076p1201>.
- [2] M. Aburas, V. Soebarto, T. Williamson, R. Liang, H. Ebendorff-Heidepriem, Y. Wu, Thermochromic smart window technologies for building application: A review, *Appl Energy*, 255 (2019) 113522, <https://doi.org/10.1016/j.apenergy.2019.113522>.
- [3] D.K. Nguyen, H. Lee, I.-T. Kim, Synthesis and Thermochromic properties of Cr-doped Al<sub>2</sub>O<sub>3</sub> for a reversible thermochromic sensor, *Materials*, 10 (2017) 476, <https://doi.org/10.3390/ma10050476>.
- [4] H. Ramlow, K.L. Andrade, A.P.S. Immich, Smart textiles: An overview of recent progress on chromic textiles, *The Journal of The Textile Institute*, 112 (2021) 152-171, <https://doi.org/10.1080/00405000.2020.1785071>.
- [5] J.H. Day, Thermochromism of inorganic compounds, *Chem. Rev.*, 68 (1968) 649-657.
- [6] L. Robertson, M. Gaudon, S. Péchev, A. Demourgues, Structural transformation and thermochromic behavior of Co<sup>2+</sup>-doped Zn<sub>3</sub>(PO<sub>4</sub>)<sub>2</sub>·4H<sub>2</sub>O hopeites, *J. Mater. Chem.*, 22 (2012) 3585-3590, <https://doi.org/10.1039/C2JM14759A>.
- [7] L.C. Robertson, M. Gaudon, S. Jobic, P. Deniard, A. Demourgues, Investigation of the First-Order Phase Transition in the Co<sub>1-x</sub>Mg<sub>x</sub>MoO<sub>4</sub> Solid Solution and Discussion of the Associated Thermochromic Behavior, *Inorg. Chem.*, 50 (2011) 2878-2884, <https://doi.org/10.1021/ic102079f>.
- [8] M. Gaudon, P. Deniard, A. Demourgues, A.E. Thiry, C. Carbonera, A. Le Nestour, A. Largeteau, J.F. Létard, S. Jobic, Unprecedented “One-Finger-Push”- induced phase transition with a drastic color change in an inorganic material, *Adv. Mater.*, 19 (2007) 3517-3519, <https://doi.org/10.1002/adma.200700905>.
- [9] M. Gaudon, C. Carbonera, A.-E. Thiry, A. Demourgues, P. Deniard, C. Payen, J.-F. Létard, S. Jobic, Adaptable thermochromism in the CuMo<sub>1-x</sub>W<sub>x</sub>O<sub>4</sub> series (0 ≤ x < 0.1): a behavior related to a first-order phase transition with a transition temperature depending on x, *Inorg. Chem.*, 46 (2007) 10200-10207, <https://doi.org/10.1021/ic701263c>.

- [10] A.-E. Thiry, M. Gaudon, C. Payen, N. Daro, J.-F. Létard, S. Gorsse, P. Deniard, X. Rocquefelte, A. Demourgues, M.-H. Whangbo, On the Cyclability of the Thermochromism in  $\text{CuMoO}_4$  and Its Tungsten Derivatives  $\text{CuMo}_{1-x}\text{W}_x\text{O}_4$  ( $x < 0.12$ ), *Chem. Mater.*, 20 (2008) 2075-2077, <https://doi.org/10.1021/cm703600g>.
- [11] Q. Dai, Y. Song, D. Li, H. Chen, S. Kan, B. Zou, Y. Wang, Y. Deng, Y. Hou, S. Yu, Temperature dependence of band gap in CdSe nanocrystals, *Chem. Phys. Lett.*, 439 (2007) 65-68, <https://doi.org/10.1016/j.cplett.2007.03.034>.
- [12] H. Serier-Brault, L. Thibault, M. Legrain, P. Deniard, X. Rocquefelte, P. Leone, J.-L. Perillon, S. Le Bris, J. Waku, S. Jobic, Thermochromism in yttrium iron garnet compounds, *Inorg. Chem.*, 53 (2014) 12378-12383, <https://doi.org/10.1021/ic501708b>.
- [13] N. Pailhé, A. Wattiaux, M. Gaudon, A. Demourgues, Correlation between structural features and vis-NIR spectra of  $\alpha\text{-Fe}_2\text{O}_3$  hematite and  $\text{AFe}_2\text{O}_4$  spinel oxides (A= Mg, Zn), *J. Solid State Chem.*, 181 (2008) 1040-1047, <https://doi.org/10.1016/j.jssc.2008.02.009>.
- [14] T. Saito, The anomalous thermal expansion of hematite at a high temperature, *Bull. Chem. Soc. Jpn.*, 38 (1965) 2008-2009.
- [15] B.T.M. Willis, H.P. Rooksby, Crystal structure and antiferromagnetism in haematite, *Proceedings of the Physical Society. Section B*, 65 (1952) 950-954.
- [16] D.S. McClure, Optical spectra of transition-metal ions in corundum, *J. Chem. Phys.*, 36 (1962) 2757-2779, <https://doi.org/10.1063/1.1732364>.
- [17] M.A. Ruiz-Preciado, A. Bulou, M. Makowska-Janusik, A. Gibaud, A. Morales-Acevedo, A. Kassiba, Nickel titanate ( $\text{NiTiO}_3$ ) thin films: RF-sputtering synthesis and investigation of related features for photocatalysis, *CrystEngComm*, 18 (2016) 3229-3236, <https://doi.org/10.1039/C6CE00306K>.
- [18] P. Jing, W. Lan, Q. Su, M. Yu, E. Xie, Visible-light photocatalytic activity of novel  $\text{NiTiO}_3$  nanowires with rosary-like shape, *Sci. Adv. Mater.*, 6 (2014) 434-440, <https://doi.org/10.1166/sam.2014.1735>.
- [19] S. Yuvaraj, V.D. Nithya, K.S. Fathima, C. Sanjeeviraja, G.K. Selvan, S. Arumugam, R.K. Selvan, Investigations on the temperature dependent electrical and magnetic properties of  $\text{NiTiO}_3$  by molten salt synthesis, *Mater. Res. Bull.*, 48 (2013) 1110-1116, <https://doi.org/10.1016/j.materresbull.2012.12.001>.
- [20] R. Tursun, Y.C. Su, Q.S. Yu, J. Tan, T. Hu, Z.B. Luo, J. Zhang, Effect of doping on the structural, magnetic, and ferroelectric properties of  $\text{Ni}_{1-x}\text{A}_x\text{TiO}_3$  (A= Mn, Fe, Co, Cu, Zn;  $x = 0, 0.05,$  and  $0.1$ ), *J. Alloys Compd.*, 773 (2019) 288-298, <https://doi.org/10.1016/j.jallcom.2018.09.133>.
- [21] R.D. Shannon, Revised effective ionic radii and systematic studies of interatomic distances in halides and chalcogenides, *Acta Crystallogr. Sec. A*, 32 (1976) 751-767, <https://doi.org/10.1107/S0567739476001551>.
- [22] A. Guiet, T.N. Huan, C. Payen, F. Porcher, V. Mougél, M. Fontecave, G.I. Corbel, Copper-Substituted  $\text{NiTiO}_3$  Ilmenite-Type Materials for Oxygen Evolution Reaction, *ACS Appl. Mater. Interfaces*, 11 (2019) 31038-31048, <https://doi.org/10.1021/acsami.9b08535>.
- [23] Y.-J. Lin, Y.-H. Chang, W.-D. Yang, B.-S. Tsai, Synthesis and characterization of ilmenite  $\text{NiTiO}_3$  and  $\text{CoTiO}_3$  prepared by a modified Pechini method, *J. Non-Cryst. Solids*, 352 (2006) 789-794, <https://doi.org/10.1016/j.jnoncrysol.2006.02.001>.
- [24] H. Rietveld, A profile refinement method for nuclear and magnetic structures, *Journal of applied Crystallography*, 2 (1969) 65-71.
- [25] W. Mokrzycki, M. Tatol, Color difference Delta E - A survey. , *Machine Graphics and Vision*, (2012)
- [26] T.F.W. Barth, E. Posnjak, The Crystal Structure of Ilmenite, *Z. Kristallogr. Cryst. Mater.*, 88 (1934) 265-270, <https://doi.org/10.1524/zkri.1934.88.1.265>.
- [27] M. Ohgaki, K. Tanaka, F. Marumo, H. Takei, Electron-density distribution in ilmenite-type crystals III. Nickel (II) titanium (IV) trioxide,  $\text{NiTiO}_3$ , *Mineralogical Journal*, 14 (1988) 133-144, <https://doi.org/10.2465/minerj.14.133>.

- [28] N.C. Wilson, J. Muscat, D. Mkhonto, P.E. Ngoepe, N.M. Harrison, Structure and properties of ilmenite from first principles, *Phys. Rev. B.*, 71 (2005) 075202, <https://doi.org/10.1103/PhysRevB.71.075202>.
- [29] H. Boysen, F. Frey, M. Lerch, T. Vogt, A neutron powder investigation of the high-temperature phase transition in NiTiO<sub>3</sub>, *Z. Kristallogr. Cryst. Mater.*, 210 (1995) 328-337, <https://doi.org/10.1524/zkri.1995.210.5.328>.
- [30] G.R. Rossman, R.D. Shannon, R.K. Waring, Origin of the yellow color of complex nickel oxides, *J. Solid State Chem.*, 39 (1981) 277-287, [https://doi.org/10.1016/0022-4596\(81\)90261-9](https://doi.org/10.1016/0022-4596(81)90261-9).
- [31] M. Llusar, E. García, M.T. García, V. Esteve, C. Gargori, G. Monrós, Synthesis and coloring performance of Ni-geikielite (Ni, Mg)TiO<sub>3</sub> yellow pigments: Effect of temperature, Ni-doping and synthesis method, *J. Eur. Ceram. Soc.*, 35 (2015) 3721-3734, <https://doi.org/10.1016/j.jeurceramsoc.2015.05.025>.
- [32] X. He, F. Wang, H. Liu, J. Li, L. Niu, Synthesis and coloration of highly dispersed NiTiO<sub>3</sub>@TiO<sub>2</sub> yellow pigments with core-shell structure, *J. Eur. Ceram. Soc.*, 37 (2017) 2965-2972, <https://doi.org/10.1016/j.jeurceramsoc.2017.03.020>.
- [33] S. Sugano, Y. Tanabe, H. Kamimura, Multiplets of transition-metal ions in crystals, Academic Press 1970.
- [34] I. Yanase, K. Oomori, H. Kobayashi, Substitution effect of V, Ca, and Ba on the thermochromic properties and thermal expansion of SrZr<sub>4</sub>(PO<sub>4</sub>)<sub>6</sub>, *Ceram. Int.*, 45 (2019) 5001-5007, <https://doi.org/10.1016/j.ceramint.2018.11.200>.
- [35] M.A. Ruiz-Preciado, A. Kassiba, A. Gibaud, A. Morales-Acevedo, Comparison of nickel titanate (NiTiO<sub>3</sub>) powders synthesized by sol-gel and solid state reaction, *Mater. Sci. Semicond. Process.*, 37 (2015) 171-178, <https://doi.org/10.1016/j.mssp.2015.02.063>.
- [36] Y. Brik, M. Kacimi, M. Ziyad, F. Bozon-Verduraz, Titania-supported cobalt and cobalt-phosphorus catalysts: characterization and performances in ethane oxidative dehydrogenation, *J. Catal.*, 202 (2001) 118-128, <https://doi.org/10.1006/jcat.2001.3262>.

### Figure captions:

**Fig. 1.** Evolution of XRD patterns of undoped NiTiO<sub>3</sub> from room temperature up to 400 °C: a) general patterns and b) zoom on the (113) peak of NiTiO<sub>3</sub> position as a function of temperature

**Fig. 2.** SEM images of undoped NiTiO<sub>3</sub> synthesized in this work: a) large view of the grains aggregates and b) close up on an aggregate evidencing the agglomeration of nano-sized grains

**Fig. 3.** Evolution of cell parameters (■) a and (●) c and c/a ratios (dotted line) as a function of temperature

**Fig. 4.** Kubelka-Munk transformed reflectance spectra collected on pure NiTiO<sub>3</sub> from RT to 400 °C

**Fig. 5.** Evolution of the colour contrast  $\Delta E$  of undoped NiTiO<sub>3</sub> as a function of temperature

**Fig. 6.** Kubelka-Munk transformed reflectivity and reflectance spectra (inset) of undoped-NiTiO<sub>3</sub> (black solid line), 2 % Cu-doped NiTiO<sub>3</sub> (brown dashed line) and 2 % Co-doped NiTiO<sub>3</sub> (green solid line) (for data colour interpretation, the reader is referred to the web version of the article)

**Fig. 7.** Evolution of  $\Delta E$  as a function of temperature for (■) undoped-NiTiO<sub>3</sub>, (●) 2 % Cu-doped NiTiO<sub>3</sub> and (▲) 2 % Co-doped NiTiO<sub>3</sub>

**List of tables:**

**Table 1.** CIELAB parameters of NiTiO<sub>3</sub> as a function of temperature, together with the corresponding pictures and their numerical images in order to highlight the colour evolution

Temperature (°C)	L*	a*	b*	Real pictures	Numerical representation
25	60.4	19.2	58.5		
50	59.4	20.3	57.8		
100	57.3	23.7	55.9		
125	56.2	25.3	54.9		
150	55.0	25.9	53.9		
175	54.0	26.9	52.7		
200	52.4	27.8	51.4		
225	51.3	28.8	50.6		
250	49.6	28.9	49.0		
275	48.6	29.1	47.7		
300	47.1	30.2	46.5		
325	46.5	30.7	46.3		
350	44.9	30.0	45.3		
375	43.9	31.2	44.3		
400	42.9	30.5	43.1		
Back to RT (30 °C)	60.5	19.3	58.8		

**Table 2.** Numerical images of undoped, Cu-doped and Co-doped NiTiO<sub>3</sub> samples showing the evolution of colour versus temperature

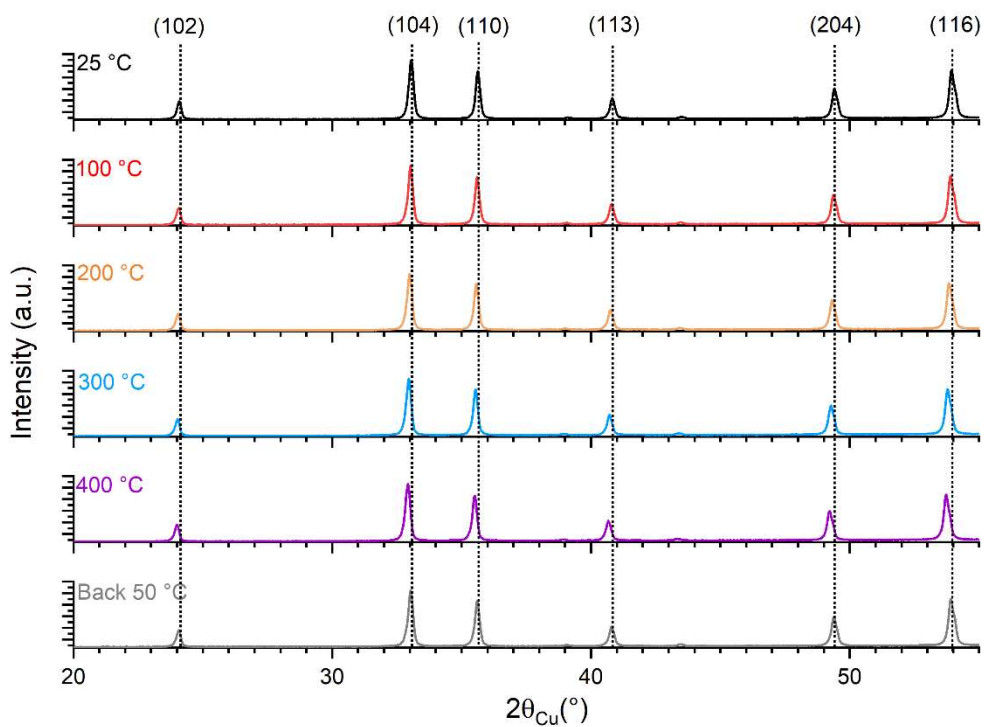
Temperature (°C)	Cu-doped	Undoped	Co-doped
20			
100			
200			
300			
400			
Back to RT (20 °C)			



**Table 3.** CIELAB parameters of  $\text{Ni}_{1-x}\text{Cu}_x\text{TiO}_3$  and  $\text{Ni}_{1-x}\text{Co}_x\text{TiO}_3$  ( $x = 0.02$ ) as a function of temperature

Temperature (°C)	Cu-doped			Co-doped		
	L*	a*	b*	L*	a*	b*
20	46.9	17.9	40.9	44.2	0.0	31.4
100	45.1	20.7	39.8	42.7	3.4	31.5
200	41.7	21.5	37.2	40.3	8.3	30.6
300	38.4	21.7	33.8	38.3	11.5	29.7
400	35.1	21.1	30.0	35.7	13.9	28.0
Back to RT (20 °C)	46.3	18.3	40.6	44.0	-0.1	32.4

a)



b)

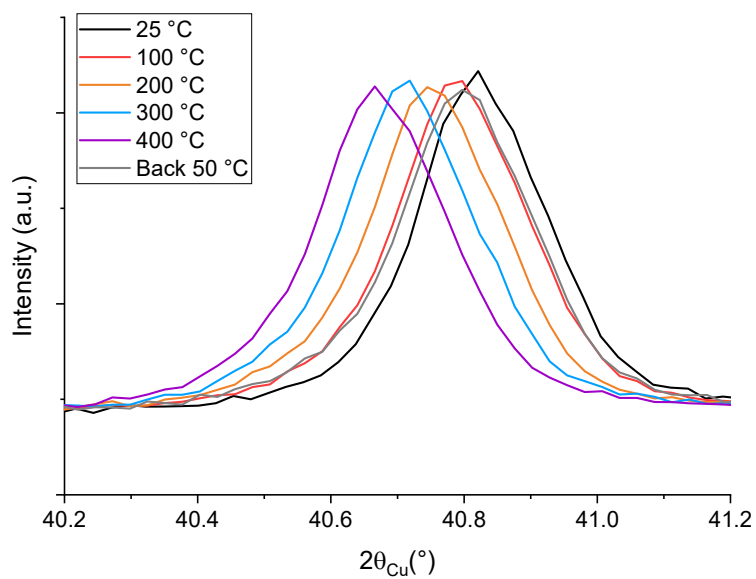


**Fig. 1.** Evolution of XRD patterns of undoped NiTiO<sub>3</sub> from room temperature up to 400 °C: a) general patterns and b) zoom on the (113) peak of NiTiO<sub>3</sub> position as a function of temperature

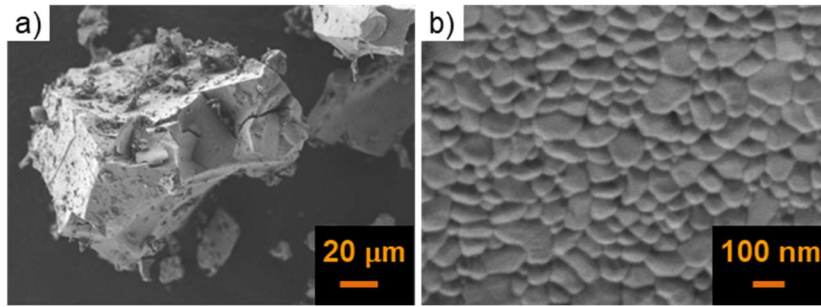


**Fig. 2.** SEM images of undoped NiTiO<sub>3</sub> synthesized in this work: a) large view of the grains aggregates and b) close up on an aggregate evidencing the agglomeration of nano-sized grains

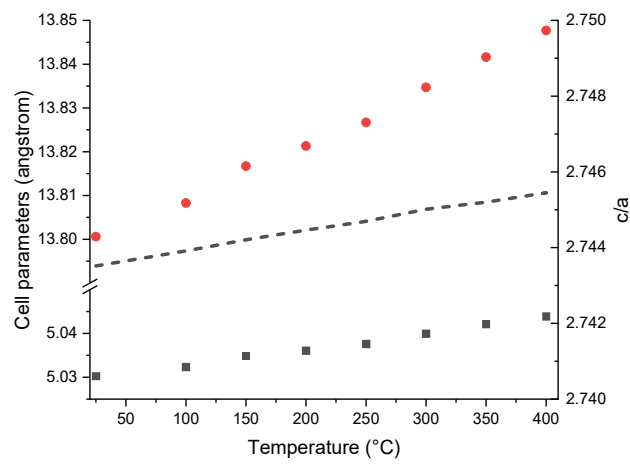


**Fig. 3.** Evolution of cell parameters (■) a and (●) c and c/a ratios (dotted line) as a function of temperature

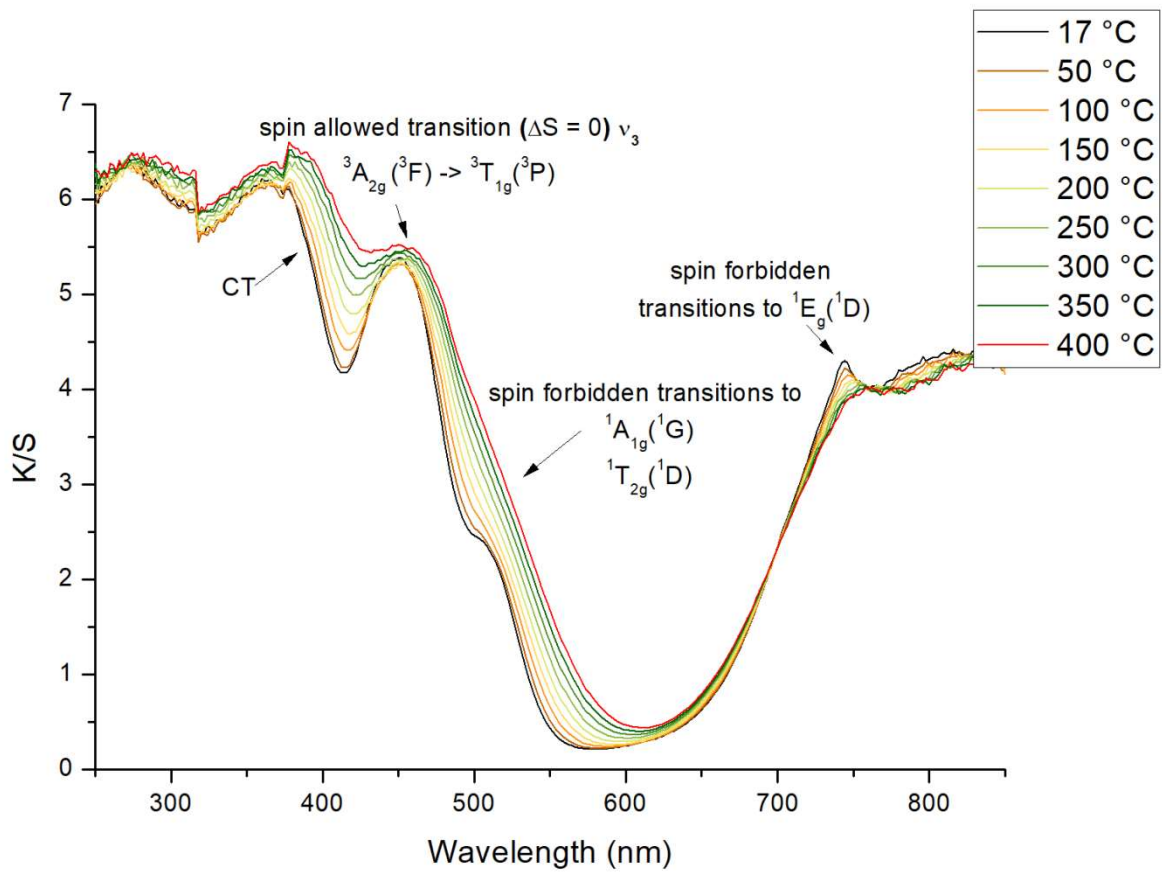


**Fig. 4.** Kubelka-Munk transformed reflectance spectra collected on pure NiTiO<sub>3</sub> from RT to 400 °C

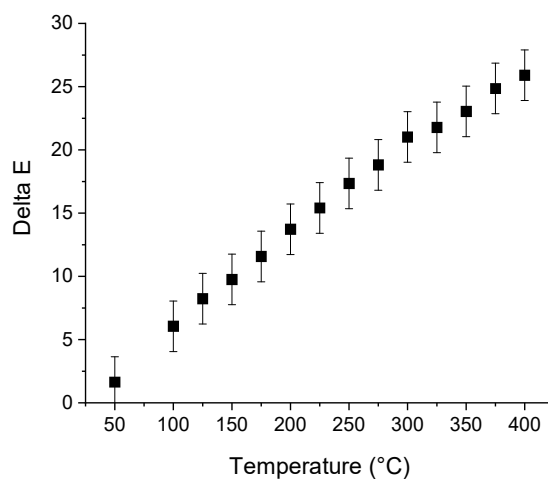


**Fig. 5.** Evolution of the colour contrast  $\Delta E$  of undoped NiTiO<sub>3</sub> as a function of temperature

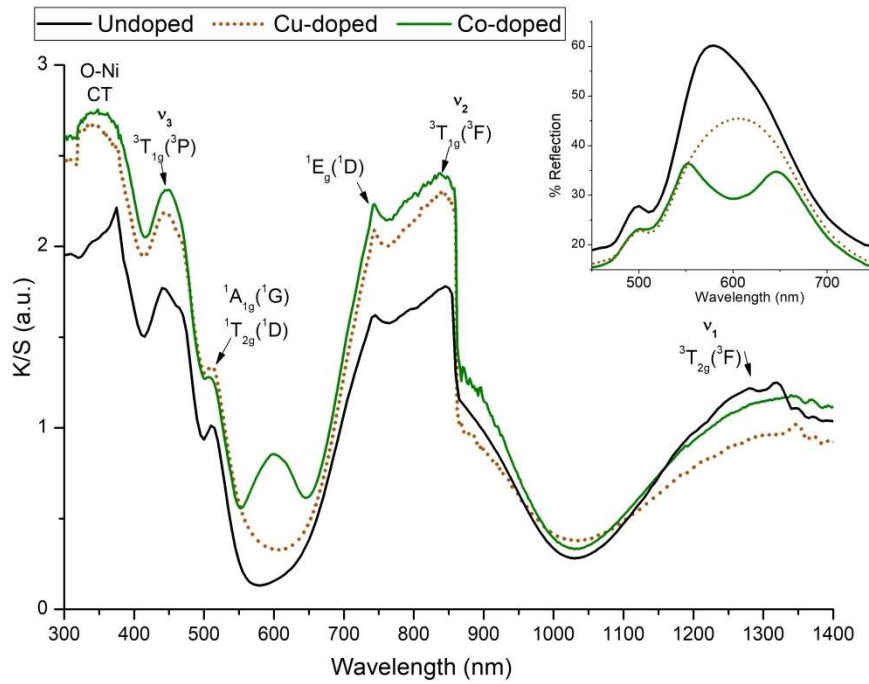


**Fig. 6.** Kubelka-Munk transformed reflectivity and reflectance spectra (inset) of undoped-NiTiO<sub>3</sub> (black solid line), 2 % Cu-doped NiTiO<sub>3</sub> (brown dashed line) and 2 % Co-doped NiTiO<sub>3</sub> (green solid line) (for data colour interpretation, the reader is referred to the web version of the article)

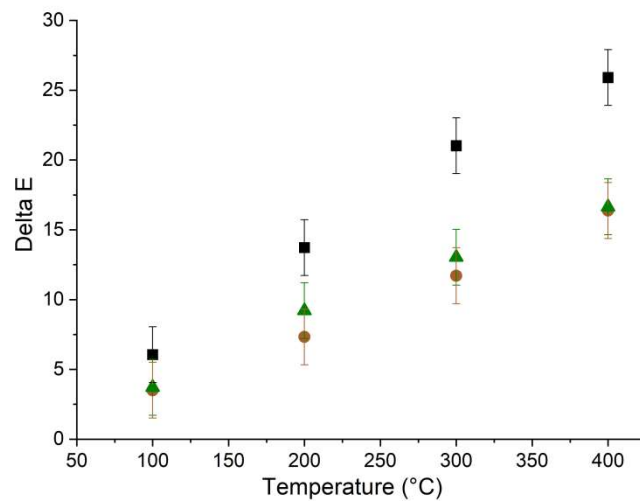
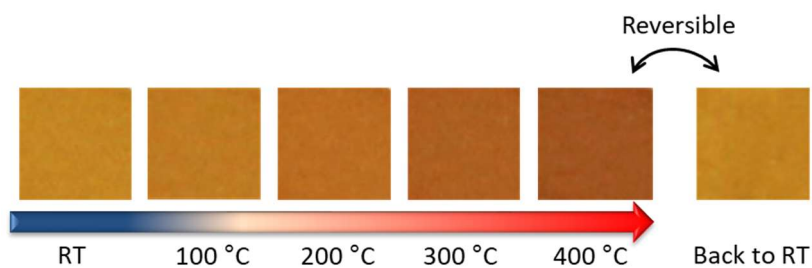


**Fig. 7.** Evolution of  $\Delta E$  as a function of temperature for (■) undoped-NiTiO<sub>3</sub>, (●) 2 % Cu-doped NiTiO<sub>3</sub> and (▲) 2 % Co-doped NiTiO<sub>3</sub>

## Highlights



Evolution of the colour of NiTiO<sub>3</sub> from room temperature up to 400 °C showing the reversible thermochromism of the material

## Supporting Information

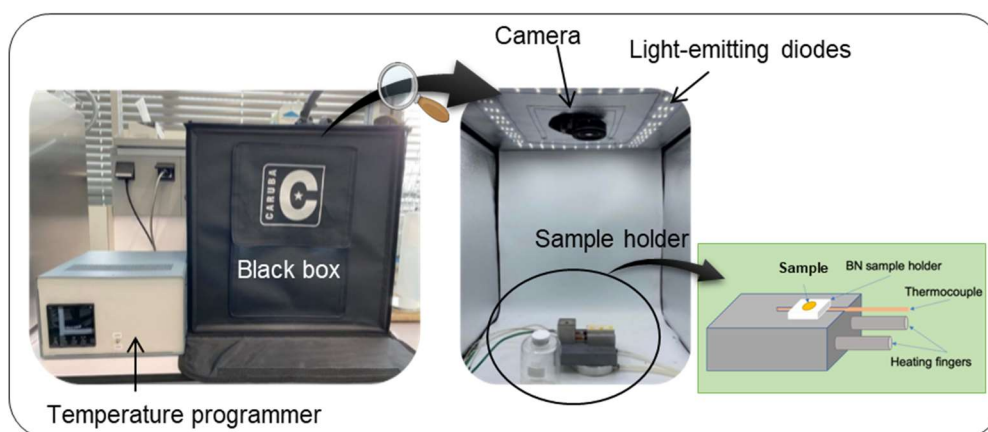


**Fig. SI.1.** Homemade set-up used for both qualitative and quantitative colour estimation versus temperature

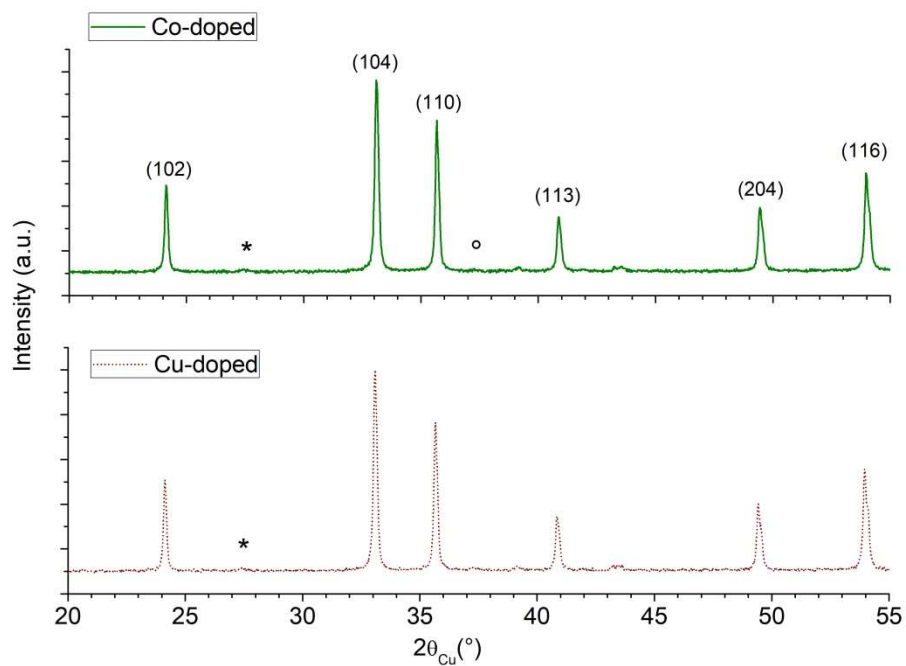


**Fig. SI.2.** XRD patterns of 2 % Cu-doped NiTiO<sub>3</sub> (brown dashed line) and 2 % Co-doped NiTiO<sub>3</sub> (green solid line) containing low amount of NiO (°) and TiO<sub>2</sub> (\*) impurities